INFRARED NON-DETECTION OF FOMALHAUT b: IMPLICATIONS FOR THE PLANET INTERPRETATION

Markus Janson[1,5], Joseph C. Carson[2], David Lafrenière[3], David S. Spiegel[4], John R. Bent[2], and Palmer Wong[2]
[1] Department of Astrophysical Sciences, Princeton University, Princeton, NJ, USA; janson@astro.princeton.edu
[2] College of Charleston, Charleston, WV, USA
[3] Department of Physics, University of Montreal, Montreal, Canada
[4] Institute for Advanced Studies, Princeton, NJ, USA
Received 2011 December 16; accepted 2012 January 12; published 2012 February 23

ABSTRACT

The nearby A4-type star Fomalhaut hosts a debris belt in the form of an eccentric ring, which is thought to be caused by dynamical influence from a giant planet companion. In 2008, a detection of a point source inside the inner edge of the ring was reported and was interpreted as a direct image of the planet, named Fomalhaut b. The detection was made at ∼600–800 nm, but no corresponding signatures were found in the near-infrared range, where the bulk emission of such a planet should be expected. Here, we present deep observations of Fomalhaut with *Spitzer*/IRAC at 4.5 μm, using a novel point-spread function subtraction technique based on angular differential imaging and Locally Optimized Combination of Images, in order to substantially improve the *Spitzer* contrast at small separations. The results provide more than an order of magnitude improvement in the upper flux limit of Fomalhaut b and exclude the possibility that any flux from a giant planet surface contributes to the observed flux at visible wavelengths. This renders any direct connection between the observed light source and the dynamically inferred giant planet highly unlikely. We discuss several possible interpretations of the total body of observations of the Fomalhaut system and find that the interpretation that best matches the available data for the observed source is scattered light from a transient or semi-transient dust cloud.

Key words: circumstellar matter – planetary systems – stars: early-type

Online-only material: color figures

1. INTRODUCTION

Direct imaging of exoplanets has been a field in rapid development over the past few years, with detections of several planets (e.g., Lagrange et al. 2010; Marois et al. 2010b) and low-mass brown dwarfs (e.g., Chauvin et al. 2005; Thalmann et al. 2009) that have been enabled by the advent of high-quality adaptive optics correction and sophisticated point-spread function (PSF) subtraction techniques. This has allowed for various kinds of characterization of such systems (e.g., Janson et al. 2010, 2011; Bowler et al. 2010; Currie et al. 2011), and opened up new domains for the types of planets that can be studied; for instance, observations within the disk gap of the transitional disk LkCa15 (e.g., Espaillat et al. 2007; Thalmann et al. 2010) using sparse aperture masking has recently revealed what could potentially be a planet in the process of forming (Kraus & Ireland 2012).

Among these discoveries, one claimed planet detection that stands out as peculiar in many ways is that of Fomalhaut b (Kalas et al. 2008, hereafter K08). The presence of a planet around Fomalhaut has been predicted on the basis of the geometry of the debris disk in the system (Kalas et al. 2005), which has a sharp inner edge and a center that is offset from that of the star. This implies that it must be eccentric, which could in turn be indicative of the presence of a planetary companion (or several) exerting a gravitational influence on the disk (e.g., Quillen 2006; Chiang et al. 2009), although alternative interpretations do exist (Jalali & Tremaine 2012). Hence, when a point source was discovered in two epochs within the disk gap (K08), with a direction of motion largely parallel to the disk edge, it was assumed that this was an image of the predicted disk-perturbing planet. However, the observed properties of the point source are hard to consolidate with such an interpretation. Unlike the other detections mentioned above, which were made at near-infrared wavelengths where young substellar objects radiate the bulk of their energy, the Fomalhaut b candidate is detected only at visible wavelengths, where the expected emission is near zero. No corresponding near-infrared radiation has so far been detected, despite several attempts (Kalas et al. 2008; Marengo et al. 2009). Several alternative interpretations of the observed properties have been made, which will be discussed in Section 4. Regardless of interpretation, it remains the case that the best way to increase our understanding of the system and test whether a planet is associated with the observed point source is to better constrain its near-infrared properties.

Motivated by this, we have performed a study with the *Spitzer Space Telescope* in order to improve the detection limits at 4.5 μm, which is the wavelength range where Fomalhaut b is expected to emit its peak flux. We describe our observational methods and data reduction in Section 2, our various data analysis approaches and results in Section 3, and discuss the implications for the Fomalhaut system in Section 4.

2. OBSERVATIONS AND DATA REDUCTION

Our observations were taken with the Infrared Array Camera (IRAC; Fazio et al. 2004) of the *Spitzer Space Telescope* as part of program 70009, and consist of eight individual runs spread over cycle 7, from 2010 August through 2011 July (see Table 1). Each run consists of 48 exposures, structured as a cycle of a 12-point Reuleaux dither pattern with four exposures per position, which enables efficient spatial oversampling and bad pixel removal. The individual exposures have integration times of 10.4 s each with an execution time of 12 s, leaving the primary saturated in individual frames. All observations were

---

Table 1
Log of Fomalhaut observations in *Spitzer* Program 70009

AOR ID	Chan.	Exp.	Frames	MJD	P.A.
40250112	4.5 μm	10.4 s	48	55416.265	254°.5
40249856	4.5 μm	10.4 s	48	55423.457	257°.6
40249600	4.5 μm	10.4 s	48	55547.666	52°.6
40249344	4.5 μm	10.4 s	48	55561.778	58°.4
40249088	4.5 μm	10.4 s	48	55571.925	62°.2
40248832	4.5 μm	10.4 s	48	55579.832	65°.0
40248576	4.5 μm	10.4 s	48	55762.480	244°.5
40250368	4.5 μm	10.4 s	48	55765.605	245°.7

taken in the 4.5 μm band where the peak flux of Fomalhaut b is expected. The observing strategy was optimized for angular differential imaging (ADI) purposes, with a large spread in telescope roll angles. Since active rotation around the optical axis of the telescope is not possible, we exploited the fact that nominal rotation occurs naturally over the course of the year and distributed the observations as uniformly over the observing cycle as the scheduling allowed. Given the observing windows for Fomalhaut, this led to observations being acquired in 2010 August and December, and 2011 January and July, with a range of position angles as summarized in Table 1.

Basic data reduction for all the observations was performed with the *Spitzer* Science Center (SSC) IRAC Pipeline (version S18.18.0), which produced basic calibrated data (BCD) frames and data quality masks for each individual exposure. We also used the post-BCD IRACproc package (version 4.3; Schuster et al. 2006) for the sole purpose of removing outliers (cosmic rays) for each frame. Subsequent steps were performed with custom procedures in IDL. An extra bad pixel removal step was introduced in order to identify and remove residual bad pixels that occurred only in single frames. This was done by identifying outliers from the median of each quadruplet of frames that were taken contiguously for a given dither position. The absolute center of the PSF in each frame was determined by cross-correlating the spider pattern with itself after a rotation by 180°. All frames were then shifted to a common center and oversampled to a pixel scale of 300 mas pixel^{-1}, after which the ADI-based PSF subtraction could commence. This procedure is based on the Locally Optimized Combination of Images (LOCI) procedure (Lafrenière et al. 2007, 2009), with adaptations to suit the new type of observational scheme and the science goals. Some similar concepts also exist within the SOSIE procedure (Marois et al. 2010a). The main aspects of the data set that distinguish it from most types of situations in which LOCI is applied are the extremely high PSF stability for space-based observations, the very large number of frames ($48 \times 8 = 384$), and the relatively small separation of the region of primary interest (compared to the PSF size, FWHM of 1″.72). Particularly the latter two factors make the data prone to substantial self-subtraction in a regular LOCI context. Since one of our main objectives in this study is to set a firm upper flux limit in case no detection would be made, we adapted the procedure in such a way as to avoid self-subtraction to a very high degree, while still maintaining a strong contrast performance. This is a conservative approach, and we note that it is entirely possible that the contrast could be even further enhanced with a more aggressive LOCI implementation. This will be a subject of future studies.

Our adapted LOCI implementation follows the following procedure: first, each frame is sequentially subjected to an individual optimized reference PSF construction and subtraction. The basic optimization area is an annulus with an inner radius of

15 pixels and an outer radius of 60 pixels, centered on the star. This optimization area is split up into pieces of approximately 9-by-9 pixels (∼1.5 FWHM). In practice, this is done in such a way that the basic annulus is split up into four annuli, each 9 pixels in width, and each annulus is split up azimuthally in such a way that an integer number of segments of equal angular width are created, and such that the length of the inner edge of the segment is as close to 9 pixels as possible. We will refer to these segments as "exclusion areas" henceforth. For each area, an individual LOCI optimization is executed where the optimization area consists of the full 15–60 pixel annulus, but with the exclusion area removed. Based on the resulting LOCI coefficients, a subtraction is then made only in the exclusion area. The resulting small area is saved to a frame which is put together piece by piece from the subtractions corresponding to the respective exclusion areas. Hence, in this procedure, the subtraction area is equal to the exclusion area and is completely non-overlapping with the optimization area. The advantage of this approach is that it becomes impossible for the algorithm to systematically fit for any companion in the data, and thus the self-subtraction will be approximately zero. The possible cost comes from the fact that we exclude the stellar PSF regions that are physically the closest to the companion, and which may therefore correlate best with the actual PSF noise at the exact position of the companion. As we will see in the testing described in Section 3, the procedure indeed works extremely well for avoiding any self-subtraction.

For the procedure described above, the reference frames are chosen from the available library of frames based on how far separated the position angles are between the subtraction frame and a given reference frame. Since we wish to ensure a very low degree of self-subtraction of any real companion, we conservatively choose that the separation must be at least 1″.72 (1 FWHM) at the inner edge of the exclusion area. This corresponds to different position angles at different separations from the star, hence the subtraction areas at larger separation typically have access to a larger number of reference frames. However, since the position angles are spread over a large range (see Table 1), every examined position has access to a sufficient number of reference frames for a very high quality PSF subtraction.

Once all frames have been subjected to the PSF subtraction, they are de-rotated to a common sky orientation where north is up and east is to the left, and collapsed into a final frame using the median of the individual frames. Another step is then performed in order to take boundary effects into account. If a real companion happens to be positioned exactly on the boundary between two or more exclusion zones, it is partially vulnerable to residual oversubtraction even in the above procedure. To overcome this effect, we perform three additional LOCI procedures in exactly the same way as described above, with only one difference: in the first additional procedure, the exclusion zones are shifted one-half step in the azimuthal direction, in the second one, they are shifted one-half step in the radial direction, and in the final one, they are shifted half a step in each direction. In this way, four different reduced frames are available to check if some companion gets fainter due to boundary effects in some of the frames and additionally allows to check for spurious features that could occur in some reductions but not in others. In this case there is a box-like artifact in two of the images but otherwise they all show nicely consistent patterns, hence for the further analysis we use the mean of the frames from the four reductions.
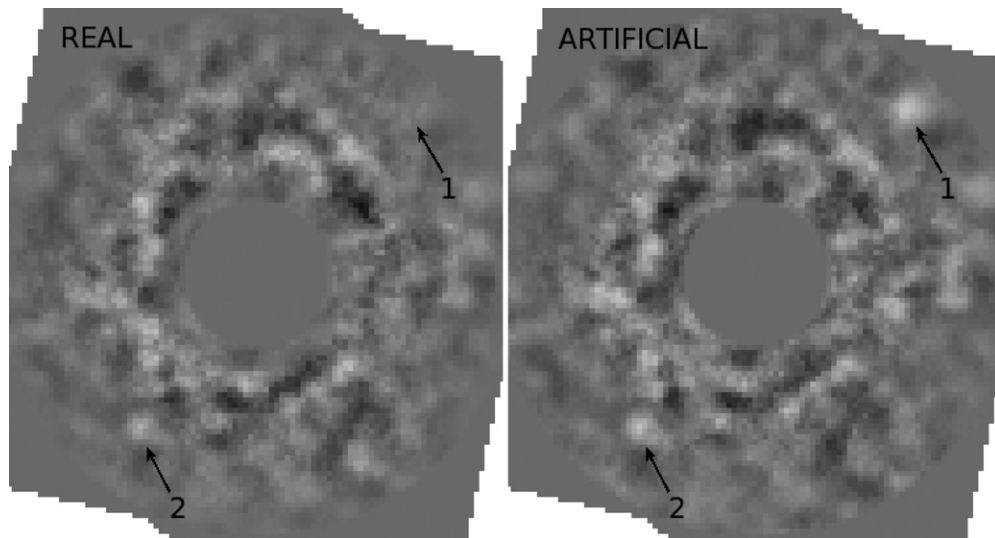
Figure 1. Final reduced image for the real data (left) and for the data with an artificial companion introduced at the expected position of Fomalhaut b (right). Arrow 1 points out the expected position of the companion based on earlier detections in the visible-light images. There is no corresponding point source seen in the real data. The artificial companion in the right-hand image passes through the data reduction without any flux loss, verifying that the non-detection is real, such that a stringent upper flux limit can be set. Arrow 2 points toward the brightest possible point source in the field. Its position is consistent with a ring-nested orbit, but the significance is too low to make any assessment of whether or not it is a real object. North is up and east is to the left in the images.

In order to evaluate the achieved contrast as a function of separation, we use the same procedure as described in Marengo et al. (2009), evaluated from the standard deviation in consecutive 1 pixel annuli. An important difference is that we always use a 5σ criterion here for our measurements, rather than 3σ as in Marengo et al. (2009). This is more stringent in the presence of speckle noise, although note also that there is a fairly close equivalence between a 5σ single-signature criterion and a 3σ double-signature criterion (Janson et al. 2008), the latter of which is relevant for the Marengo et al. (2009) data.

3. RESULTS AND ANALYSIS

We show the final reduced image in Figure 1 and the corresponding sensitivity limits in Figure 2, where we also plot the expected brightnesses for planets of a few different masses at ages of 200 and 400 Myr. A very substantial improvement in contrast performance is achieved with our LOCI implementation, with an order of magnitude improvement in flux detectability compared to the conventional ADI reduction in Marengo et al. (2009), and with a more stringent detection criterion. No signature is found at the position where Fomalhaut b would be expected. Hence, we estimate an upper limit (5σ) at the relevant position based on the standard deviation in a 7-by-7 pixel box ($\sim$1.2 FWHM on the side). This gives an upper limit of 16.7 mag, which corresponds to 38.8 μJy, again more than an order of magnitude improvement over previous data.

In order to test that the non-detection is real and not an effect of any unexpected oversubtraction in the LOCI procedure, we make a full reduction following the exact same procedure as described in the previous section, except we also introduce a faint artificial companion (a Gaussian with 1″.72 FWHM) in all the pre-LOCI frames, at the expected position of Fomalhaut b, with a flux of 57 μJy (this corresponds to an effective temperature of $\sim$250 K, or equivalently 0.5–1 M_{jup} at 200 Myr and 1–2 M_{jup} at 400 Myr). The artificial companion passes through the LOCI reduction entirely unaffected, with the same measured flux in the final frame as the flux that was put in within the error bars, and is clearly visible at 7σ confidence in
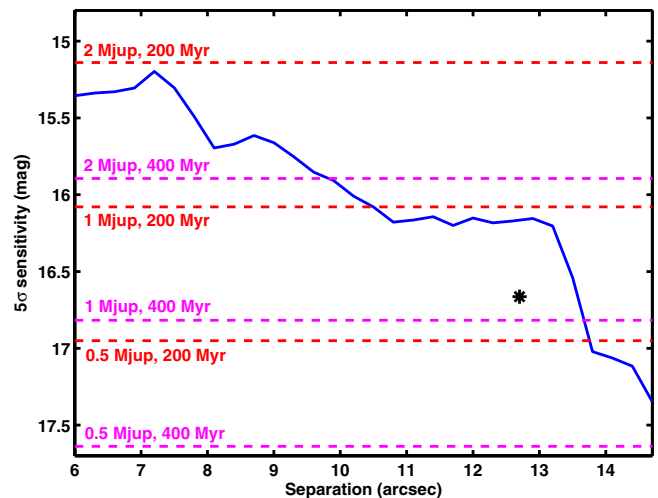

Figure 2. Sensitivity limit as function of separation from Fomalhaut. The solid line is the azimuthally averaged sensitivity profile. There is a bump around 12″ due to concentrated noise at some ranges of position angles. The expected position of Fomalhaut b from the visible wavelength range detections is in a cleaner part of the image space, and the local sensitivity at this position is shown by the black asterisk. Also plotted as dashed lines are the expected brightnesses for planets with a few different combinations of mass and age, according to models from Spiegel & Burrows (2012).

(A color version of this figure is available in the online journal.)

the final frame (see Figure 1). Note that the introduction of a new feature in the data affects the LOCI reduction itself—since the artificial companion exists in most reference frames as an additional feature that has to be fit for by the algorithm, the fit quality will in general be slightly worse on average. Since the extent of the companion is small with respect to the optimization area and it is faint with respect to the stellar PSF, the effect is small but noticeable as a marginally higher general noise level in the final reduced frame. In summary, the procedure described here validates that the non-detection is real, and thus the upper flux limit is relevant.

We show our upper limit in Figure 3, along with other upper limits from the literature at various wavelengths, as
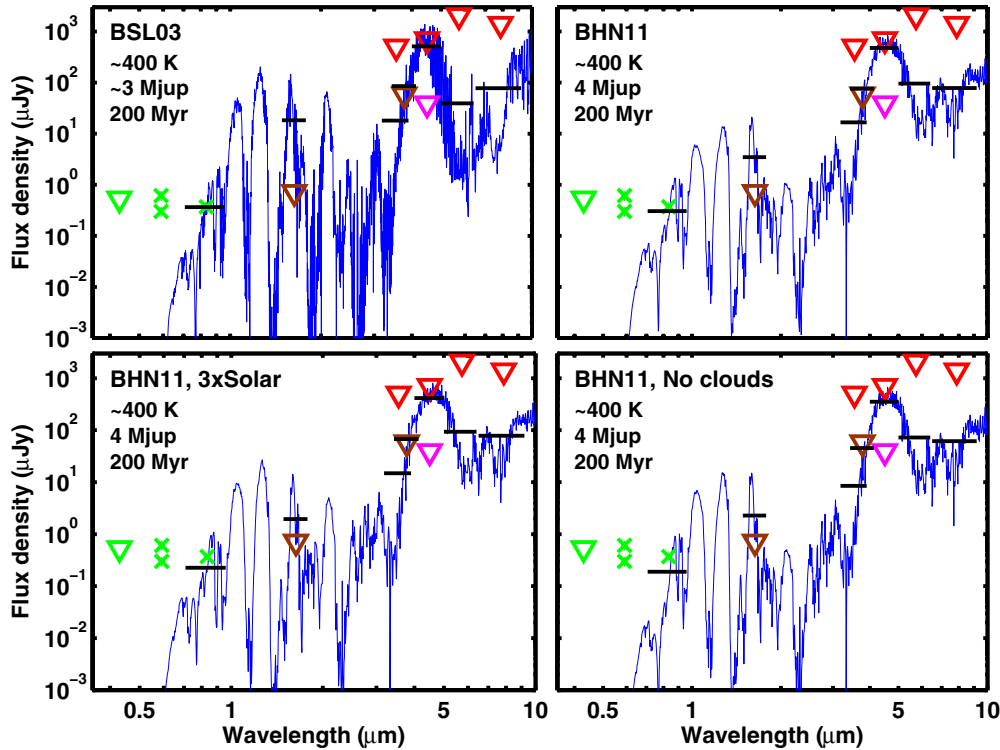
Figure 3. Model comparisons to the observational data for a ∼400 K atmosphere (∼2–3 M_{jup} at ∼200 Myr for BSL03, 4 M_{jup} at 200 Myr for BHN11). The solid line in each panel is the model spectrum, and the black lines are the corresponding fluxes in the respective photometric bands. Crosses mark detections and triangles mark upper limits. *Hubble Space Telescope* (*HST*) data points from K08 are in green and Keck/Gemini data points from K08 are in brown. Note that the error bars at F606W and F814W are smaller than the sizes of the symbols. Red symbols are *Spitzer* upper limits from Marengo et al. (2009). Our new upper limit from *Spitzer* is the magenta triangle. Upper left: a BSL03 model. Upper right: a BHN11 model with patchy clouds and solar composition. Lower left: a BHN11 model with patchy clouds and increased metallicity. Lower right: a BHN11 model with solar composition and a cloud-free atmosphere. Models in this effective temperature range are required to produce an adequate amount of flux in F814W, but they are typically inconsistent with the upper flux limits in *H* band and/or *L′* band, and always fully inconsistent with the upper limit at 4.5 μm.

(A color version of this figure is available in the online journal.)

well as the detection values in the visual wavelength range. We also compare these values with various theoretical models. One model spectrum is from Burrows et al. (2003, henceforth BSL03), corresponding to a 2–3 M_{jup} planet (interpolated between 2 M_{jup} and 5 M_{jup} to match the flux value at F814W[6]) at ∼200 Myr. As noted in K08 and Marengo et al. (2009), this model is similar to, e.g., the Fortney et al. (2008) model except in *H* band where the BSL03 flux is higher. It can be seen from the comparison to the data that in the context of this model, a thermal flux interpretation is entirely inconsistent with both the non-detection in *H* band and our non-detection in the IRAC 4.5 μm channel. The *H*-band flux is strongly model dependent as it is sensitive to uncertainties in opacity and the treatment of clouds. However, by contrast, the 4.5 μm flux is very insensitive to these effects, and varies only very marginally across different models. To show this, we use newer models from Spiegel & Burrows (2012) based on Burrows et al. (2011, henceforth BHN11), which has improved opacities and cloud treatment, and also includes a set of entirely cloud-free models for comparison.

By using these new models and including clouds, it is possible to suppress the *H*-band flux to a significant extent (though typically still not quite to a sufficient extent for a non-detection to be consistent with thermal flux in F814W).

However, this is not the case at 4.5 μm. The flux remains very stable for a constant effective temperature (typically ∼400 K for these model comparisons), regardless of how the clouds are treated including the cloud-free case, independently of opacity treatment and also of specific metallicity (the BHN11 models provide both solar and super-solar metallicity cases). We conclude that the effective temperatures required to get any substantial contribution of thermal flux to the observed F814W data point are simply inconsistent with the non-detection at 4.5 μm.

In order to comply with the upper limit at 4.5 μm, we need effective temperatures in the range of ∼200 K or lower, corresponding to, e.g., 1 M_{jup} at 400 Myr (see Figure 4). As a side point, this latter age would correspond to a new but so far unpublished estimate (E. Mamajek 2010, private communication) which is a little older than the mean estimate of 200 Myr used in K08 and Marengo et al. (2009). Here, we do not make any assessment of the relative credibility of these two estimates, but simply remark that it has no real relevance for the spectral comparisons we are performing here. The main factor (beyond cloud treatment and opacity) that affects the spectral energy distribution (SED) is the effective temperature. The mass to which this temperature corresponds depends on the age and vice versa, but this has little impact on the spectrum, especially for the small discrepancy in age that we are concerned with here. Hence, as long as we do not actually try to determine the mass, we do not need to assess which of 200 Myr or 400 Myr is the

---

[6] F606W and F814W are filters for the Advanced Camera for Surveys on the *Hubble Space Telescope*, centered on wavelengths of ∼600 and ∼800 nm, respectively.
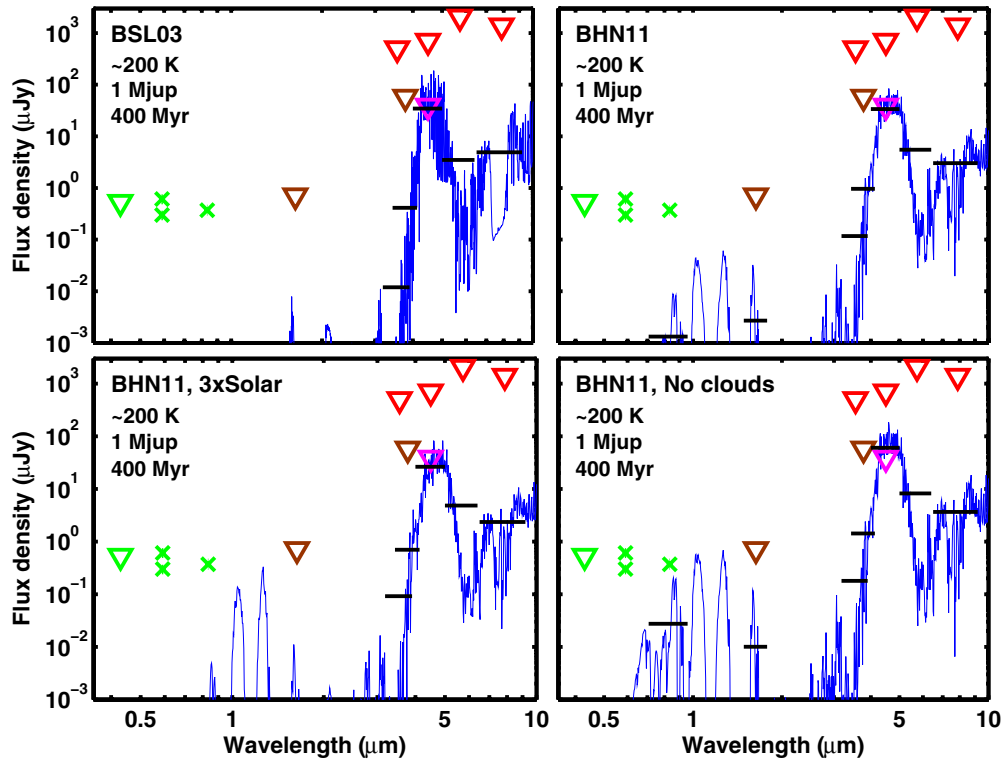
Figure 4. Model comparisons to the observational data for a ∼200 K atmosphere (1 M_{jup}, 400 Myr). The symbols have the same meaning as in Figure 3. Upper left: a BSL03 model. Upper right: a BHN11 model with patchy clouds and solar composition. Lower left: a BHN11 model with patchy clouds and increased metallicity. Lower right: a BHN11 model with solar composition and a cloud-free atmosphere. These models are marginally consistent with the upper flux limit at 4.5 μm, but predict one to several orders of magnitude too little flux to be consistent with thermal radiation in F814W.

(A color version of this figure is available in the online journal.)

better estimate. While on this note, it is worth pointing out that hot/warm/cold-start models are of no significant relevance to this discussion, since convergence will have occurred at these ages and masses, regardless of initial entropy (Spiegel & Burrows 2012).

For the colder models required to match the 4.5 μm upper flux limit, virtually all fluxes at shorter wavelengths are lost, and there is no way to match the F814W point with any thermal flux. The closest case is the extreme case of a completely cloud-free atmosphere and solar metallicity, but also in this case the flux is more than an order of magnitude too small (see Figure 4). Increasing metallicity has the effect of decreasing flux at 800 nm compared to 4.5 μm, hence decreasing metallicity could have the opposite effect. However, Fomalhaut A has a super-solar metallicity with a mean measured value of 0.3 dex in a compilation of literature values in Soubiran (2010). Fomalhaut b should have an equal or larger metallicity—thus, adjusting the metallicity is not a feasible route toward reaching consistency with the observational data.

Based on the above results and considering the further aspects of the collected body of observations of Fomalhaut as will be discussed in detail in Section 4, it is highly unlikely that the observed flux at visible wavelengths has any direct connection to the suspected giant planet that might shepherd the debris disk of Fomalhaut and force it into an eccentric state (Kalas et al. 2005). In this context, and considering our very strong detection limits, it is interesting to assess whether this shepherding planet (what might be referred to as the "real" Fomalhaut b) can be seen in our images. Since the shepherding planet can be as low in mass as 0.5 M_{jup} (Chiang et al. 2009), it is fully plausible that it could remain undetected in our images if the age is as

old as 400 Myr, and since its orbit covers a range of projected separations, it can also hide in some parts of the orbit even if the mass is slightly higher. However, we do cover a very large fraction of its possible parameter space, and it is noteworthy that the brightest possible point source in the field with a significance of 4.3σ is in fact located at a position that would be consistent with a ring-nested orbit (arrow 2 in Figure 1). However, the fact that the possible point source is not at a 5σ confidence level obviously means that more data or an even further improved PSF reduction would be necessary in order to test its validity.

4. DISCUSSION

In this section, we discuss in detail how our non-detection at 4.5 μm affects the interpretation of Fomalhaut b, and what can be deduced about the system from the full body of existing data. The data points that exist for the detected point source in K08 are two detections in the F606W filter from 2004 to 2006 and one detection in the F814W filter from 2006. These data points are shown in Figures 3 and 4. Note that the object is variable between 2004 and 2006. This is not a small effect; in fact, it corresponds to a change in brightness (dimming) of a factor two, at a confidence of 8σ. This is the same level of confidence as, e.g., the second-epoch F606W detection of the point source altogether. Hence, to the extent that we can trust the data at all, we must consider this variability as a real effect, and it needs to be accounted for in a comprehensive interpretation of the object. In addition to these data, a third epoch *HST* observation has also been acquired but has not yet been published at the time of writing (P. Kalas 2010, private communication). There are also upper flux limits from non-detections in a range of bands in

Kalas et al. (2008): F435W, H, CH4S, CH4L, and L', and upper limits at 3.6, 4.5, 5.8, and 8.0 μm from *Spitzer* (Marengo et al. 2009), the second of which we improve on in this article.

There are two main lines of interpretation of the point source in K08, only one of which actually includes any flux from a planet. In this scenario, the flux at F814W originates from the thermal emission of a planet, which has to be close to a mass of $\sim$3 $M_{\rm jup}$ in order to fit the data point assuming an age of 200 Myr (e.g., Burrows et al. 2003; Fortney et al. 2008). This is however poorly consistent with the rest of the available data. Most obviously, it is a factor 20–40 brighter in F606W than expected in such a scenario. In order to explain the F606W data in terms of brightness and variability, K08 infer a hypothesis of Hα accretion on the planet. Given that this would require gas accretion at the same rate of a few Myr old T Tauri stars like GQ Lup (accretion rate calculated in the supplemental material of K08), whereas Fomalhaut is 200–400 Myr and has no other known signs of gas anywhere in the system, we consider this hypothesis highly unlikely.

Aside from this, there is the issue that a $\sim$3 $M_{\rm jup}$ companion should also be detectable in the near-infrared. This was an issue already in K08, where the *H*-band flux predicted by theoretical models was significantly higher than the upper limit from observations and became an even larger issue given the *Spitzer* data published by Marengo et al. (2009), where the additional limits at larger wavelengths provided very little opportunity for any flux to remain undetected from such a companion. As was shown in the previous section, our new *Spitzer* data now provide even much tighter constraints on the thermal emission hypothesis and provide the opportunity to conclusively address this issue. We find that any thermally emitting companion responsible for the F814W flux (effective temperatures of $\sim$400 K, e.g., 2–3 $M_{\rm jup}$ at 200 Myr) would have emitted more than an order of magnitude more flux at 4.5 μm than our 5σ upper limit, regardless of the choice of theoretical models. Conversely, any companion that thermally emits radiation at 4.5 μm at levels comparable to our upper limit (effective temperatures of $\sim$200 K, e.g., 1 $M_{\rm jup}$ at 400 Myr) would emit at least an order of magnitude too little flux at F814W to explain the observations, and for most realistic model parameters (e.g., any inclusion of clouds) the flux would be even much smaller. Hence, we can firmly exclude the hypothesis that any of the observed flux in K08 actually originates from a giant planet.

Given that the SED of the K08 point source can be interpreted as having a reasonable match to the stellar SED, it seems more likely that what is seen in the K08 images is some form of reflected or scattered radiation from the star. Given the large effective area that is required for this, the only plausible origin for reflected/scattered radiation is dust. Hence, it is likely that we are seeing a concentration of dust, which may or may not be associated with a planet. We will discuss some dust-related interpretations in the following: first, we will consider the hypothesis of an optically thick disk around a giant planet. This is the second preferred scenario in K08 and requires a disk radius of at least $\sim$20 $R_{\rm jup}$ (for the case of high albedo; larger for the case of low albedo). It may not be unreasonable that circumplanetary rings start out with such properties. However, it might also be argued that the age of the Fomalhaut system of 200–400 Myr should have provided adequate time for moons to form and excavate the disk, leaving only rings of a much smaller effective size. Regardless of whether the optically thick disk scenario is fundamentally realistic or not, there are several reasons why this scenario is inconsistent with the existing data. One very important constraint is that such a disk cannot account for the factor two variability observed in F606W. Furthermore, the spin of the star has been recently measured with interferometry (Le Bouquin et al. 2009). If the spin of the star is aligned with the plane of the disk, this means that the fainter western side is closer to us than the brighter eastern side. Although this is opposite to what would be expected for purely forward-scattering dust, it is shown in Min et al. (2010) to be consistent with the scattering behavior of large dust grains. If it is indeed the case that the western side of the disk is closer to us, and the K08 point source orbits within the disk, then it follows that the object is located between the parent star and Earth, in the radial direction. It would be very difficult for an optically thick disk to reflect large amounts of light to Earth under such circumstances.

In addition to these points, another important argument against the involvement of a giant planet (which also applies to the thermal emission case discussed above) is the orbit of the object. The third epoch astrometric measurement implies a ring-crossing orbit for the point source (P. Kalas 2010, private communication). Although this is not yet published, it would not be surprising given the previously published data, because, in fact, already the first two epochs are inconsistent with an orbit that traces the edge of the ring, at a $\sim$2σ level (the direction is largely consistent with such an orbit, but the speed is not). This is pointed out by Chiang et al. (2009), who do not put a large emphasis on this fact, as they argue that the error bars are probably underestimated. However, we note that this is diametrically opposite to the interpretation of the astrometric errors in K08, where it is concluded that they are an upper limit to the real error (K08, supplemental material). A ring-crossing orbit would be inconsistent with an association of the point source to a giant planet, as it would strongly affect the geometry of the disk, which results in an upper mass limit of $\sim$10 $M_{\rm Earth}$ (Kennedy & Wyatt 2011).

In the context of an upper limit of $\sim$10 $M_{\rm Earth}$ in mass, we note that one way to suppress the 4.5 μm flux with respect to shorter wavelengths is to consider hotter temperatures and smaller surfaces. Effective temperatures higher than $\sim$200–400 K that we have considered thus far are not reasonable for isolated objects at the system age, particularly for smaller (and thus lower-mass) objects than Jupiter-class planets. However, following intense bombardment of planetesimals, rocky protoplanets may acquire molten surfaces and reach effective temperatures of $\sim$1000–3000 K over brief periods of time (Miller-Ricci et al. 2009). Hence, the possibility that the observed light-source could be a hot collisional afterglow of a $\leqslant$10 $M_{\rm Earth}$ object should not be dismissed out of hand. Still, it would probably be difficult to reproduce all the observed data points in such an interpretation, particularly the detection in F606W, and the simultaneous non-detections in *H* band and at 4.5 μm. The Miller-Ricci et al. (2009) models do not cover the full relevant wavelength range, but if we consider, for example, a planet of 10 $M_{\rm Earth}$ and 1.8 $R_{\rm Earth}$ and work from pure blackbody considerations, we can establish that the brightness temperature required to reproduce even the lowest of the F606W data points (0.30 μJy) is more than 1500 K, whereas the upper limits in *H* band (0.71 μJy) and at 4.5 μm (38.8 μJy) both require brightness temperatures of $\sim$700 K or less. We consider that future modeling efforts would be worthwhile to examine whether these conditions and the rest of the flux limits can all be simultaneously fulfilled, but for the purpose of our discussion here, we simply treat it as an option that cannot be categorically excluded. On balance, it should be

noted that an observation of this type of scenario is probably rather unlikely, for several reasons, including the fact that it is expected to last over timescales of $\sim10^4$ yr for the case of a thin atmosphere, very short compared to the age of Fomalhaut. The timescale can be extended if the atmosphere is thickened and clouds are included, but the observable brightness temperature decreases accordingly. As a side note, if clouds were involved, they could possibly account for the variability in F606W in this scenario.

Given the SED of the point source and its variability, along with the considerations above, the perhaps most plausible way to consistently explain the observed properties of the K08 point source is through a cloud of dust, which is either transient or has a transient component. There are two possible scenarios associated with such an interpretation that have been suggested in the literature. In one scenario, the observed point source is a residual (gradually dispersing) dust cloud from a recent planetesimal collision. We certainly know that such collisions should occur frequently in the Fomalhaut system, given that they are the very origin of dust in debris disks. This scenario is mentioned by K08, who argue against it based on the fact that such collisions should be much more common within the actual ring feature than just outside of it where the point source is observed, hence the relative probability to observe it where it is observed should be low. This is certainly true, but we note that there is a clear selection effect involved—due to the high visual brightness of the ring and the speckle-like nature of the noise, any number of equivalent events that hypothetically do happen within the ring feature would be likely to pass unnoticed. One might also hypothetically imagine that the cloud is in the present position for some specific dynamical reason, for instance if the material is trapped in resonance with a giant planet situated elsewhere.

The second scenario is essentially the same as the first, but involves a central rocky/icy object with a mass less than $\sim10\,M_{\rm Earth}$, to which a swarm of planetesimals is gravitationally bound. Collisions between these planetesimals produce the observed dust. We consider both of these scenarios to be reasonable within the constraints set by the data, and simply conclude that the K08 point source is well consistent with a transient or semi-transient dust cloud, which may or may not be gravitationally bound to a central object of planetary mass. With regards to the fact that the point source has been frequently referred to as a directly imaged planet in the literature, we note that this is incompatible with the observational evidence, for two independent reasons: (1) although it cannot be formally excluded, there is insufficient evidence to support that there is any compact object of planetary mass associated with the point source altogether. (2) Even if such an object is present, in several of our considered scenarios we do not observe any photons from this object itself, hence it cannot be established that it has been directly imaged.

5. CONCLUSIONS

In this paper, we have presented observations performed with *Spitzer*/IRAC in the $4.5\,\mu$m band for the purpose of trying to detect thermal emission from Fomalhaut b. A new LOCI-based PSF subtraction scheme was implemented to achieve high contrast with minimal companion flux loss, which enabled an order of magnitude improvement in contrast-limited sensitivity with respect to previous efforts. The non-detection of any flux at the expected position can therefore be used to provide strong constraints on the underlying physics of the point source seen at visible wavelengths. In particular, we find that there is almost certainly no direct flux from a planet contributing to the visible-light signature. This, in combination with the existing body of data for the Fomalhaut system, strongly implies that the dynamically inferred giant planet companion and the visible-light point source are physically unrelated. This in turn implies that the "real" Fomalhaut b still hides in the system. Although we do find a tentative point source in our images that could in principle correspond to this object, its significance is too low to distinguish whether it is real or not at this point.

Concerning the visible-light point source, its underlying physics is unclear, but the only hypothesis that can be shown to reasonably fit all existing data is an optically thin dust cloud, which is transient or has a transient component. If this interpretation is valid, the cloud may or may not be physically bound to a central object in the super-Earth mass regime.

REFERENCES

Bowler, B., Liu, M., Dupuy, T., & Cushing, M. 2010, ApJ, 723, 850
Burrows, A., Heng, K., & Nampaisarn, T. 2011, ApJ, 736, 47
Burrows, A., Sudarsky, D., & Lunine, J. I. 2003, ApJ, 596, 587
Chauvin, G., Lagrange, A.-M., Zuckerman, B., et al. 2005, A&A, 438, 29
Chiang, E., Kite, E., Kalas, P., Graham, J. R., & Clampin, M. 2009, ApJ, 693, 734
Currie, T., Burrows, A., Itoh, Y., et al. 2011, ApJ, 729, 128
Espaillat, C., Calvet, N., D'Alessio, P., et al. 2007, ApJ, 670, 135
Fazio, G. G., Hora, J. L., Allen, L. E., et al. 2004, ApJS, 154, 10
Fortney, J., Marley, M., Saumon, D., & Lodders, K. 2008, ApJ, 678, 1419
Jalali, M. A., & Tremaine, S. 2012, MNRAS, in press (arXiv:1110.4551)
Janson, M., Bergfors, C., Goto, M., Brandner, W., & Lafrenière, D. 2010, ApJ, 710, L35
Janson, M., Carson, J., Thalmann, C., et al. 2011, ApJ, 728, 85
Janson, M., Reffert, S., Brandner, W., et al. 2008, A&A, 488, 771
Kalas, P., Graham, J. R., Chiang, E., et al. 2008, Science, 322, 1345
Kalas, P., Graham, J., & Clampin, M. 2005, Nature, 435, 1067
Kennedy, G. M., & Wyatt, M. C. 2011, MNRAS, 412, 2137
Kraus, A. L., & Ireland, M. J. 2012, ApJ, 745, 5
Lafrenière, D., Marois, C., Doyon, R., & Barman, T. 2009, ApJ, 694, 148
Lafrenière, D., Marois, C., Doyon, R., Nadeau, D., & Artigau, E. 2007, ApJ, 660, 770
Lagrange, A.-M., Bonnefoy, M., Chauvin, G., et al. 2010, Science, 329, 57
Le Bouquin, J.-B., Absil, O., Benisty, M., et al. 2009, A&A, 498, 41
Marengo, M., Stapelfeldt, K., Werner, M. W., et al. 2009, ApJ, 700, 1647
Marois, C., Macintosh, B., & Veran, J.-P. 2010a, Proc. SPIE, 7736, 52
Marois, C., Zuckerman, B., Konopacky, Q., Macintosh, B., & Barman, T. 2010b, Nature, 468, 1080
Miller-Ricci, E., Meyer, M. R., Seager, S., & Elkins-Tanton, L. 2009, ApJ, 704, 770
Min, M., Kama, M., Dominik, C., & Waters, L. B. F. M. 2010, A&A, 509, 6
Quillen, A. C. 2006, MNRAS, 372, L14
Schuster, M. T., Marengo, M., & Patten, B. M. 2006, Proc. SPIE, 6270, 65
Soubiran, C., Le Campion, J.-F., Cayrel de Strobel, G., & Caillo, A. 2010, A&A, 515, 111
Spiegel, D. S., & Burrows, A. 2012, ApJ, 745, 174
Thalmann, C., Carson, J., Janson, M., et al. 2009, ApJ, 707, L123
Thalmann, C., Grady, C. A., Goto, M., et al. 2010, ApJ, 718, L87